STAR NOTE # 351

The Electromagnetic Calorimeter and Shower Maximum Detector Performance In 1997 Testbeam Run At BNL

S. Bennett[1],W. Christie[2], T. Cormier[1], A.A. Derevschikov[3], G. Epply[4], O.A. Grachov[5], T. Hallman[2], G. Igo[6], T. LeCompte[7], B. Llope[4], Yu.A. Matulenko[3], J. Riso[1], V.L. Rykov[1], K.E. Shestermanov[8], H. Spinka[7], S. Trentalange[6], O.D. Tsai[5], D. Underwood[7], A. Vander Molen[9], A.N. Vasiliev[10], G. Westfall[9], A. Yokosawa[7]

Abstract

We present measurements of EMC and SMD responses for electrons and hadrons/muons from the 1997 testbeam. The experimental results are compared to GEANT simulations.

[1]Wayne State University, Detroit, Michigan 48202
[2]Brookhaven National Laboratory, Upton, New York 11973
[3]Institute of High Energy Physics, Protvino, Moscow Region 142284, Russia
[4]Rice University, Houston, TX 77251
[5]Institute of High Energy Physics, Protvino, Moscow Region 142284, Russia and Wayne State University, Detroit, Michigan 48202
[6]California,University of (Los Angeles), Los Angeles, CA 90095-1547
[7]Argonne National Laboratory, Argonne, Illinois 60439
[8]Institute of High Energy Physics, Protvino, Moscow Region 142284, Russia and Brookhaven National Laboratory, Upton, New York 11973
[9]Michigan State University, East Lansing, MI 48824-1321
[10]Institute of High Energy Physics, Protvino, Moscow Region 142284, Russia and Argonne National Laboratory, Argonne, Illinois 60439

1 Introduction

The goal of the 1997 testbeam run was to study the performance of a double sided Shower Maximum Detector (SMD) prototype and a sampling Electromagnetic Calorimeter (EMC) prototype with scintillator megatiles. Negative beam at AGS test beam-line of momenta 0.5, 1, 2 and 5 Gev/c, mostly pions with admixture of muon and electron was used.

The Setup during the May'97 run at BNL was as follows:

- looking downstream along the beam, first, there were two trigger scintillator counters - East and West.
- the next detector was a gas Cherenkov counter;
- after the Cherenkov counter, Big Veto counter with two phototubes, called Up and Down, was in the beam line. A hole was about of $5\times6\,\mathrm{cm}^2$;
- the next two detectors were scintillator hodoscopes, X- and Y- planes. Each hodoscope consisted of 16 strips of 6 mm wide. These strips were overlapping to form 31 channels of 2 mm wide each, except two outer ones, which were 4 mm wide;
- after the Hodoscopes, Small Veto with a hole of $1\times1\,\mathrm{cm}^2$, and a Finger counter in the hole with the size of 1 cm by 1 cm, were in the beam line;
- at the end of the beam line was the EMC prototype, consisting of 8 towers (one tower was readout with a depth segmentation) and the gaseous double sided SMD prototype placed inside the EMC after approximately $5X_o$.

2 The Geometry of the Electromagnetic Calorimeter and Shower Maximum Detector

The EMC geometry used in this RUN was a Scintillator-Lead calorimeter consisting of 8 towers. The EMC segmentation was $\Delta\eta\times\Delta\phi = 0.05$ it covered $0.05 \leq \eta \leq 0.25$ and azimuthal angle $-3^\circ \leq \phi \leq 3^\circ$.

The calorimeter stack consisted of 21, 5 mm thick, scintillator (BICRON 404A) tiles with 20 lead-sheets of the same thickness in between the tiles. In front of the first tile there was a 19 mm thick aluminum plate. The SMD was placed after the 6th Sc tile and before the 6th lead plate, at a depth of approximately $5X_o$.

The SMD was a gaseous double sided multi-wire proportional chamber. The front and back plates consisted of a 2 mm thick G10 printed circuit board with cathode strips on its surface. An Al plate 7.6 mm thick, with a rib in the η direction, separated the two gaseous volumes. The 6.1 mm thick ionization sensitive volume between the Al plate and front and back G10 board was filled with the 90% Ar plus 10% CO_2 gas mixture. The readout from the SMD was from signal cathode strips in the front plane, X-direction and in back plane, Y-direction. The SMD strip widths were 14 mm and 18 mm for X and 13.41 mm for Y. The results of analysis presented in this paper are for 14 mm strips only. Strip pitches were 14.63 mm and 14.53 mm, correspondingly. One of the strips had an Fe55 radioactive source on it to monitor high voltage stability in the SMD.

The initial particles have been directed toward the EMC block at various angles. The data with exposition at 90 degrees only were analysed, and the results are included in this Note.

3 Electrons or Hadrons/Muons selection in EMC/SMD

In the results presented below we've used the following criteria for event selection. For electrons :

1) Not Fe55 event - the response of the strip $X1$ in SMD, where Fe55 source was sitting, must be outside of a Fe55 spectrum.

1) Good Trigger - responses from both West and East trigger counters must be inside of their signal spectra.

2) Big Veto - responses from both Up and Down veto counters must be below their signal spectra.

3) The signal from the Cherenkov counter must be above the threshold.

4) Good Hodoscope - we demanded that in each of the two hodoscope plane (sometimes only X- plane to save statistics), there should be either the signal in only one channel, or in two and only two adjacent overlapping rods.

5) SMD Boundary Cut - the center of gravity of a shower in SMD must not be closer than 35 mm from the SMD instrumented boundary (selection with the use of hodoscopes).

6) Not Fe55 event - the response of the strip $X1$ in SMD, where Fe55 source was sitting, must be outside of a Fe55 spectrum.

For hadrons/muons :

1,2 and 4,5,6) are the same as for electrons ;

3) Cherenkov counter response must be below the threshold of the electron spectrum.

To get an impression how these applied cuts worked in terms of statistics, a typical example for electrons is presented in Table 1.

Table 1. Efficiencies of the electron selection.

	Run51 (2 GeV)	Run53 (5 GeV)
Number of events	1	1
1)Not Fe55 events	0.996	0.996
2)Good Trigger	0.870	0.870
3)No Big Veto	0.866	0.869
4)Electron in Cheren.	0.069	0.016
5)Good Hodoscope	0.0069[1]	0.0018
6)SMD Boundary Cut	0.0055	0.0014

The measured fractions of electrons in the beam of various momenta was as follows:

0.5 GeV – 38%; 1 GeV – 21%; 2 GeV – 7.6%; 5 GeV – 1.8%.

The typical statistics per run was 1 to 3×10^6 events. After all cuts, the number of survived electron events was about a few thousand.

[1]Here we used a requirement to have a good hit in both X- and Y- planes of the Hodoscopes. A suppression factor is about 10.

4 "Minimum-ionizing" particles in the EMC

Many charged hadrons (along with small admixtures of electrons and muons) will be produced in every collision at RHIC. In the central region covered by the STAR Barrel EMC (BEMC), these are mostly pions. When striking the BEMC, a significant fraction ($\sim 30-40\%$) of high energy charged hadrons do not deposit a large amount of energy via strong interactions, instead depositing ~ 20 MeV of energy in the calorimeter's 21 scintillator layers due largely to electromagnetic ionization. In this note, we will loosely call these hadrons (and muons too) "Minimum Ionizing Particles" (MIPs) producing "MIP-hits" in the BEMC towers. For the relativistic particles, the position of the "MIP-peak" is nearly independent of momentum and particle species. This, along with the high yield of charged hadrons, makes it attractive to explore the feasibility of using high energy MIPs for the equalization, calibration, and continuous tracking of the stability of the BEMC tower's gains. In Fig. 1, the experimental distributions of the signals from Tower 2 at four different momenta of the beam are shown. For all four momenta, the hits have been selected in the same area of the size $2 \times 3\, cm^2$, far away from the tower's edges. These spectra include the contributions of all particles in the beam but electrons, which have been rejected using the Cherenkov counter. No other cuts to select events have been applied. Apparently, MIP-peaks dominate in these spectra and cannot be lost or confused with something else. To determine the positions of the MIP-peaks, the "Gaussian + polynomial" fits have been used[1]. The "most probable signals" (parameter P2) obtained from these fits and the relative widths of the peaks (ratio P3/P2) are shown in Table 2. One can observe that the variation of the MIP-peak position in the momentum range from 0.5 to 5 GeV/c is about 2%. In the momentum interval of 1-2 GeV/c, which is the most important for the BEMC calibrations using MIPs, the measured variation is even smaller, just $\sim 0.5\%$[2].

[1]Since χ^2 in these fits are not good enough, we are looking now for better functions to replace Gaussians.

[2]Actually, the motion of the MIP-peak position in this data cannot be considered as purely due to the momentum change. The uncontrolled particle compositions might also be different at different momenta. Moreover, as it is follows from the analysis of Sec. 6, the uncontrolled time-variations of the channel's gains could be as large as $\sim 3.5-4\%$

Table 2. Momentum dependence of the MIP-peak position in Tower 2.

Momentum, GeV/c	Position, P2	Width, P3/P2, %
0.5	62.6 ± 0.2	14.3
1	62.3 ± 0.1	16.9
2	61.7 ± 0.1	16.5
5	63.1 ± 0.1	17.9

It was found at the analysis stage that MIP-hits appear to represent a convenient tool to study some important characteristics of the calorimeter. Using MIP-hits, we measured the non-uniformity of the EMC response over the tower surface. It turned out to be $\pm 5\%$ (from maximum to minimum) within one quarter of the Tower 2, covered by the hodoscope. Time non-stability (including electronics) is 5% for 21 hours of running time, and 3.5% for 5 hours within these 21.

5 EMC performance

The measured EMC energy in Tower 2 in ADC counts at each nominal energy is shown in Fig.2. Fitting with a Gaussian we calibrated Tower 2. The calibration coefficient was found to be about 5 MeV/ADC channel.

The EMC energy resolution is presented in Fig.3. It is consistent with $\sigma(E)/E = (1.5 \pm 0.33)\% + (15 \pm 0.52)\%/\sqrt{E}$. GEANT gave us $(0.81 \pm 0.27)\% + (16.96 \pm 0.48)\%/\sqrt{E}$. The results of GEANT simulations on energy resolutions are presented in Table 3.

Table 3. GEANT simulated resolution: (1) is for $\sigma(E_d)/E_d$ where $E_d = \sum_{i=1}^{21} \epsilon_i$ is the energy deposited by an electron in 21 scintillator tiles; (2) is for $\sigma(L)/L$ where $L = \sum_{i=1}^{21} y_i \times \epsilon_i$, and y_i is the measured mean light yield from i-th tile; (3) is for $\sigma(S)/S$ where S is the Tower's 2 signals, accounting the measured y_i and the statistics of photoelectrons at the mean over 21 tiles yield of ~ 3.5 phe/MIP/tile; (3/1) is for ratios $(\sigma(S)/S)/(\sigma(E_d)/E_d)$.

E GeV	1	2	3	3/1
0.5	19.6 ± 0.5	21.5 ± 0.5	23.5 ± 0.6	1.20 ± 0.04
1.0	14.0 ± 0.3	16.4 ± 0.4	18.1 ± 0.4	1.30 ± 0.04
2.0	10.3 ± 0.2	12.4 ± 0.3	13.8 ± 0.4	1.34 ± 0.05
5.0	6.4 ± 0.1	8.0 ± 0.2	8.5 ± 0.2	1.33 ± 0.04
7.0	5.6 ± 0.1	6.9 ± 0.2	7.0 ± 0.1	1.25 ± 0.04

Energy dependence of energy resolution for 3 above mentioned cases as a result of a fit of the data is given by the following formula:

$1 - (0.37 \pm 0.20)\% + (13.70 \pm 0.36)\%/\sqrt{E}$

$2 - (1.40 \pm 0.23)\% + (14.77 \pm 0.40)\%/\sqrt{E}$

$3 - (0.81 \pm 0.27)\% + (16.96 \pm 0.48)\%/\sqrt{E}$

The energy dependence of EMC response is presented in Fig.4. We have not found a deviation from linearity more than 2% in the 0.5 to 2 GeV region. At 5 GeV the EMC energy response is 13% lower than expected. This non-linearity might come from the non-uniformity of the tile light output. For Tower 2 it turns out that this non-uniformity was large, up to a factor of four (see Fig.5). The reasons for this might be fiber damage, poor quality splicing of green and transparent fibers, or defects in the grooves for the fibers. GEANT simulations showed that the effect of this particular non-uniformity is opposite to the effect observed in the data. Instead of -13% it has given +10% at 5 GeV (see Fig.6). We have done an analytic calculation on average showers (using the Rossi parameterisation [1]), and get a consistent answer (+8%). We concluded that the phototube base might be the cause of this non-linearity. Also the energy resolution at 5 GeV, which turned out to be better than the anticipated one, pointed out at this effect. It turned out that to make this May'97 run real, we had to borrow Russian phototubes PMT-115M together with bases from our IHEP colleagues at D0. There were no other phototubes and bases available for the STAR EMC prototype that we could secure in time. We suppose that the non-linearity observed at the Test run was connected with these bases.

6 SMD performance

The SMD response in ADC counts for the front plane measured at each electron beam energy is shown in Fig.7. It was about the same for the back plane, though energy deposition in the back plane (MEAN value over the ADC range) was 10% less than in the front plane.

The electronics scale was about 1.8 MeV per ADC channel in equivalent electromagnetic energy of the beam electron. This electronics scale was about

19 eV per ADC channel in terms of the primary ionization in the SMD gas volume, as determined from the position of the Fe55 (5.9 keV) peak. We should notice that the MIP energy deposit was ~ 1.6 keV in one plane of the SMD.

Energy dependence in SMD energy response is presented in Fig.8. The data are fitted by straight line. We have found that SMD is linear within 8% in X-plane and within 5% in Y-plane.

The SMD energy resolution is presented in Fig.9. It is consistent with $\sigma(E)/E = 12\% + 86\%/\sqrt{E}$. Energy resolution in the back plane is a few percent (3-4%) worse than in the front plane.

The coordinates of the "logarithmic weighted center of shower" in the SMD, were calculated, using the formulae [2]:

$$X_c = \frac{\sum_i X_i W_i}{\sum_i W_i}; \quad \text{with} \quad W_i = max[0, W_0 + ln(E_i/E_{tot})]; \tag{1}$$

where E_i is the energy deposited under the i-th strip; X_i is the position of the center line of the i-th strip; E_{tot} is the total energy deposition in the SMD; $W_0 = 2.0$. The SMD position resolution is presented in Fig.10. It is consistent with $\sigma(x) = 2.4\,mm + 5.6\,mm/\sqrt{E}$ for the front plane and $\sigma(x) = 3.2\,mm + 5.8\,mm/\sqrt{E}$ for the back plane.

The degradation of the spatial resolution in the back plane is due to the presence of the low Z materials (Al, gas) in front of this plane. This effect was investigated in detail during the study of our previous prototype SMD [3].

The use of the logarithmic method is motivated by the exponential falloff of the shower profile. This corrects the deficient behaviour of the linear weight approach where a centrally hit element will contain most of the energy and will systematically pull the position calculation.

Fig.11 shows the systematic pull in the position calculation in the case of a linear weight for the 5 GeV showers. The uniform distribution of the impact parameter across the strip surface in the case of linear weighting in the expression for the center of gravity leads to a systematic shift to the geometrical center of the strip (in region ± 2.5 mm from the center of the strip). The logarithmic method appears to be free of this problem.

SMD efficiency to detect electrons and hadrons/muons are presented in Fig.12. The efficiency was defined as the ratio of events with non zero signal in the SMD planes to the total number of triggers. At 0.5 GeV the SMD

has about a 60% electron efficiency. It grows up to 90% at 1 GeV and 100% at 2 GeV and higher. Electron efficiencies for both planes are approximately equivalent.

7 SMD shower profiles

SMD shower profiles for the front plane, for four energies, are presented in Table 4 and in Fig. 13. Distance from the position of the electron hit in mm is in the first column. In the following columns there are relative energy deposits in %. The integral over a shower profile at any energy was 100%.

The dependence of the shower width on energy is presented in Fig.14. The shower width gets narrower as the energy is increased.

Table 4. The measured electron shower profiles in the SMD at four energies. In the first column there is a distance from the position of the electron hit. In the following columns there are relative energy deposits.

Dist. mm	E=0.5 GeV %	E=1 GeV %	E=2 GeV %	E=5 GeV %
0-5	29.5 ± 0.9	35.7 ± 0.8	39.2 ± 0.5	42.3 ± 0.5
5-10	22.3 ± 0.8	24.8 ± 0.6	25.4 ± 0.5	25.6 ± 0.4
10-15	18.5 ± 0.8	17.2 ± 0.5	17.2 ± 0.4	15.8 ± 0.4
15-20	10.0 ± 0.5	8.2 ± 0.3	6.9 ± 0.3	6.9 ± 0.3
20-25	5.9 ± 0.4	4.2 ± 0.2	3.4 ± 0.2	3.5 ± 0.2
25-30	4.7 ± 0.4	3.3 ± 0.2	2.7 ± 0.2	2.3 ± 0.1
30-35	3.1 ± 0.3	2.3 ± 0.2	1.9 ± 0.2	1.5 ± 0.1
35-40	2.3 ± 0.3	1.9 ± 0.2	1.2 ± 0.1	0.9 ± 0.1
40-45	1.9 ± 0.3	1.3 ± 0.1	1.0 ± 0.1	0.8 ± 0.1
45-50	1.9 ± 0.3	1.0 ± 0.1	0.8 ± 0.1	0.5 ± 0.06

8 Comparison of observed shower profiles with GEANT

GEANT simulated shower profiles for four energies are presented in Table 5 and in Fig.15. The format of the data is the same as in Table 4. The ratios of the GEANT to the experimental shower profiles are presented in Table 6.

One observes that the GEANT shower profile is narrower than the experimental one in the energy range from 0.5 GeV to 5 GeV. In the central bin of 0-5 mm from the position of the electron's hit, it is higher than the experimental profile by (45-20)%, depending on energy. Both energy deposits are equal at around 10 mm. In the "tail" from 30 to 50 mm, GEANT predicted relative energy deposits that are a factor of 2.5-1.5 smaller compared to the experiment. The GEANT profile gets closer to the experimental one when the energy is increased from 0.5 to 5 GeV (see Fig.16).

Table 5. GEANT simulated electron shower profiles in the SMD at four electron energies.

Dist. mm	E=0.5 GeV %	E=1 GeV %	E=2 GeV %	E=5 GeV %
0-5	43.1 ± 1.2	46.3 ± 0.8	48.4 ± 0.6	50.9 ± 0.5
5-10	26.3 ± 1.0	30.0 ± 0.8	29.4 ± 0.5	29.9 ± 0.5
10-15	14.7 ± 0.8	10.8 ± 0.5	10.3 ± 0.3	8.9 ± 0.2
15-20	7.1 ± 0.6	5.2 ± 0.3	4.6 ± 0.2	4.1 ± 0.1
20-25	2.7 ± 0.3	2.7 ± 0.2	2.6 ± 0.2	2.2 ± 0.1
25-30	2.3 ± 0.3	1.5 ± 0.2	1.7 ± 0.1	1.5 ± 0.1
30-35	1.3 ± 0.2	1.4 ± 0.2	1.1 ± 0.1	1.1 ± 0.1
35-40	1.2 ± 0.2	0.9 ± 0.1	0.8 ± 0.1	0.7 ± 0.1
40-45	0.8 ± 0.2	0.5 ± 0.1	0.6 ± 0.1	0.5 ± 0.1
45-50	0.4 ± 0.1	0.7 ± 0.1	0.5 ± 0.1	0.4 ± 0.04

Table 6. The ratios of GEANT simulated relative energy deposits (Table 5) to the measured ones (Table 4).

Dist. mm	E=0.5 GeV	E=1 GeV	E=2 GeV	E=5 GeV
0-5	1.46 ± 0.06	1.30 ± 0.04	1.23 ± 0.02	1.20 ± 0.02
5-10	1.18 ± 0.07	1.21 ± 0.04	1.16 ± 0.03	1.17 ± 0.03
10-15	0.79 ± 0.04	0.63 ± 0.03	0.60 ± 0.02	0.56 ± 0.02
15-20	0.71 ± 0.06	0.64 ± 0.05	0.66 ± 0.04	0.59 ± 0.04
20-25	0.46 ± 0.06	0.65 ± 0.06	0.76 ± 0.05	0.61 ± 0.05
25-30	0.49 ± 0.08	0.46 ± 0.07	0.63 ± 0.06	0.63 ± 0.05
30-35	0.43 ± 0.07	0.63 ± 0.10	0.60 ± 0.08	0.73 ± 0.08
35-40	0.54 ± 0.11	0.45 ± 0.07	0.70 ± 0.10	0.73 ± 0.09
40-45	0.41 ± 0.06	0.41 ± 0.08	0.56 ± 0.12	0.56 ± 0.08
45-50	0.23 ± 0.12	0.65 ± 0.11	0.66 ± 0.08	0.76 ± 0.11
30-50	0.41 ± 0.04	0.50 ± 0.04	0.63 ± 0.04	0.68 ± 0.04

9 e/h-rejection with EMC and SMD

For any particular momentum which, in the STAR experiment, is measured in the tracking system, the electron signals are concentrated in relatively narrow intervals around mean values, while the energy deposits from hadrons are spread over wide ranges. Therefore, by selecting only the hits within some distance of the electron peak of the known momentum, the EMC itself represents a quite powerful tool for electron/hadron separation. Hadron rejection, using only the EMC, for 3 different electron detection efficiencies, are presented in Fig.17 as function of energy. For 80% electron efficiency, the EMC itself rejects hadrons by 4 times at 0.5 GeV and by 30 times at 5 GeV.

One of the advantages of the final double-sided design of the SMD is the independent measurement of the primary ionization in two gas samples inside the EMC. Large fluctuations of the ionization in thin layers of gas can cause the ionization from a single minimal ionization particle to be comparable to that of an electromagnetic shower of a few GeV. This leads to degradation of the SMD electron/hadron rejection power. In the case of two independent gas samples, the probability of such an event is obviously smaller

A study of electron/hadron rejection in the EMC and SMD can be carried out by several methods. We do not pretend in this paper to compare the

results of all of these methods. We just show one concrete approach to estimate the scale of e/h rejection values.

First, separate cuts on energy deposition are made for the front and back planes of the SMD such that 90% of the survive. Fig.18(a) gives the entire sample for electrons and hadrons (Run53, Test97, 5 GeV) as well as the SMD cuts applied to preferentially select electrons. For muons and hadrons which don't interact in the first $5X_o$ of the EMC, there should be no dependence of the ionization in the front and back planes of the SMD on the incoming particle momentum.

Fig.18(b) shows the amplitude spectra in the EMC for the entire data sample (open histogram) and surviving events after applying the SMD cuts described above (cross hatched histogram). The rejection power of the SMD itself is comparable to the rejection power of the longitudinal non-segmented EMC, and close to 30:1 for this particular energy, with an electron detection efficiency of 80%.

While the e/hadron selection, using the EMC and SMD separately, are pretty much correlated, they are not exactly the same. For example, the SMD is virtually insensitive to hadron showers which start beyond the SMD depth in the EMC. To some extent, the EMC and SMD sensitivity is also different for the hadron showers starting before the SMD, but fully developed after the SMD. As a result, the rejection power of the combined detector (EMC/SMD) is higher than of either of them separately.

Fig.18(c) shows the distribution of the ratio of the sum of the strip logarithmic weights over energy deposition in the EMC for the front (SumWsmdX) vs back (SumWsmdY) planes of the SMD for the events surviving the SMD energy cuts. The above variables were calculated as follows:

$$SumWsmdX \propto \frac{\sum_i Wx_i}{E_{emc}}(GeV^{-1}); \;\; SumWsmdY \propto \frac{\sum_i Wy_i}{E_{emc}}(GeV^{-1}); \quad (2)$$

where Wx_i and Wy_i were logarithmic weights for the strips in the front and back SMD planes determined using the formulae (1), with the parameter $W_0 = 2.0$. The electron events are mostly located in the 'head' of the 'comet', while the hadron events are in the halo. In this figure, the marked area in the 'head' of the 'comet' contains the 80% of all electrons from the original data sample. Fig.18(d) shows the amplitude spectra in the EMC for the surviving events (the hatched one). The overall rejection power for the detector is $(1.2 \pm 0.1) \times 10^2$ for 80% electron efficiency. In the energy range from 0.5

to 5 GeV the information from the SMD improves the rejection power of the non-segmented EMC by about a factor of 3.

10 Conclusion

What have we learned from the 1997 BNL test run for the EMC and SMD in the 0.5 to 5 GeV energy range?

1. Charged hadrons and muons, which do not have a strong interaction in the EMC, deposit in its 21 scintillator tiles about the same energy as 300 MeV electrons. For the momentum range 0.5-5 GeV/c and within the experimental uncertainty of 3-4%, the MIP-peak position in the EMC does not depend on the energy of the AGS negative test beam.

2. It has been found that, apparently, MIP-hits are a convenient and virtually "free" tool for detailed study of many important EMC characteristics, namely: light leakage from tower-to-tower, nonuniformity of the light collection across the towers, and time stability of the EMC channel's gains.

3. The measured non-uniformity of the light collection across the EMC prototype's towers was $\sim \pm 5\%$ which is in a good agreement with the bench tests. The variation of the EMC gains with time was 5% for 21 hours, and 3.5% for 5 hours within these 21 hours.

4. The EMC response was linear within 2% accuracy in the 0.5 to 2 GeV energy range. There was a 13% non-linearity at 5 GeV. The GEANT simulations, using the measured numbers for the light yield from the tile, have shown that the variation of the light output from tile-to-tile does not explain the observed nonlinearities. We suppose that the non-linearity observed in the test run was connected with the bases.

5. The EMC energy resolution $\sigma(E)/E$ was $1.5\% + 15\%/\sqrt{E}$. GEANT gave $1\% + 17\%/\sqrt{E}$.

6. We have found that the SMD energy response is linear within 8% in the X-plane and within 5% in the Y-plane.

7. The SMD energy resolution $\sigma(E)/E$ was $12\% + 86\%/\sqrt{E}$.

8. The SMD position resolution was $\sigma(x) = 2.4\,mm + 5.6\,mm/\sqrt{E}$ for the front plane and $\sigma(x) = 3.2\,mm + 5.8\,mm/\sqrt{E}$ for the back plane.

9. In the SMD back plane compared to the front plane : - energy deposit was 10% less ; - energy resolution was 3-4% worse ; - position resolution was 15% worse.

10. The SMD efficiency to detect electrons increases as the energy increases. In both planes it was 60% at 0.5 GeV, 90% at 1 GeV, achieved eventually 100% at 2 GeV and stayed flat at higher energy. SMD efficiency for hadrons/muons increased for the front plane from 20% at 0.5 GeV up to 70% at 5 GeV, and for the back plane from 40% at 0.5 GeV up to 80% at 5 GeV.

11. The width of the electromagnetic shower in the SMD decreased as the energy increased.

12. GEANT SMD shower profile was narrower than the experimental one, but got closer to the experimental profile as the energy increased.

13. The EMC gave hadron rejection from 4 to 30 times at 0.5 to 5 GeV at 80% electron detection efficiency. Additional information from the SMD increased this rejection in about 3 times.

We would like to thank Dmitry Denisov from D0 , who gave us the phototubes and bases for the test run at BNL in May'97.

References

[1] B. Rossi, High Energy Particles, Prentice-Hall, Inc., Englewood Cliffs, NJ, 1952.

[2] T. C. Awes et al. Nucl. Instr. and Meth. **A311** (1992) 130.

[3] S. A. Akimenko et al. Nucl. Instr. and Meth. **A365** (1995) 92.

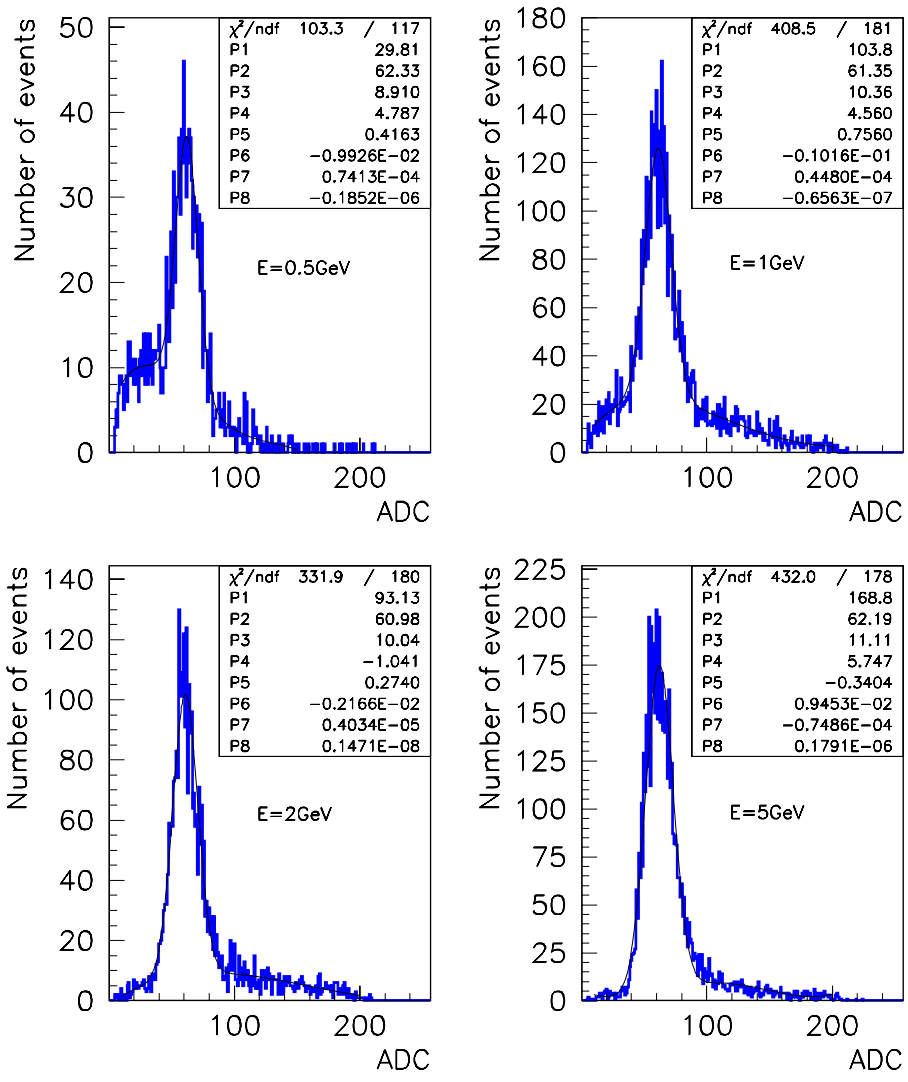

Figure 1: MIP-peaks in Tower 2 at 0.5, 1, 2 and 5 GeV/c.

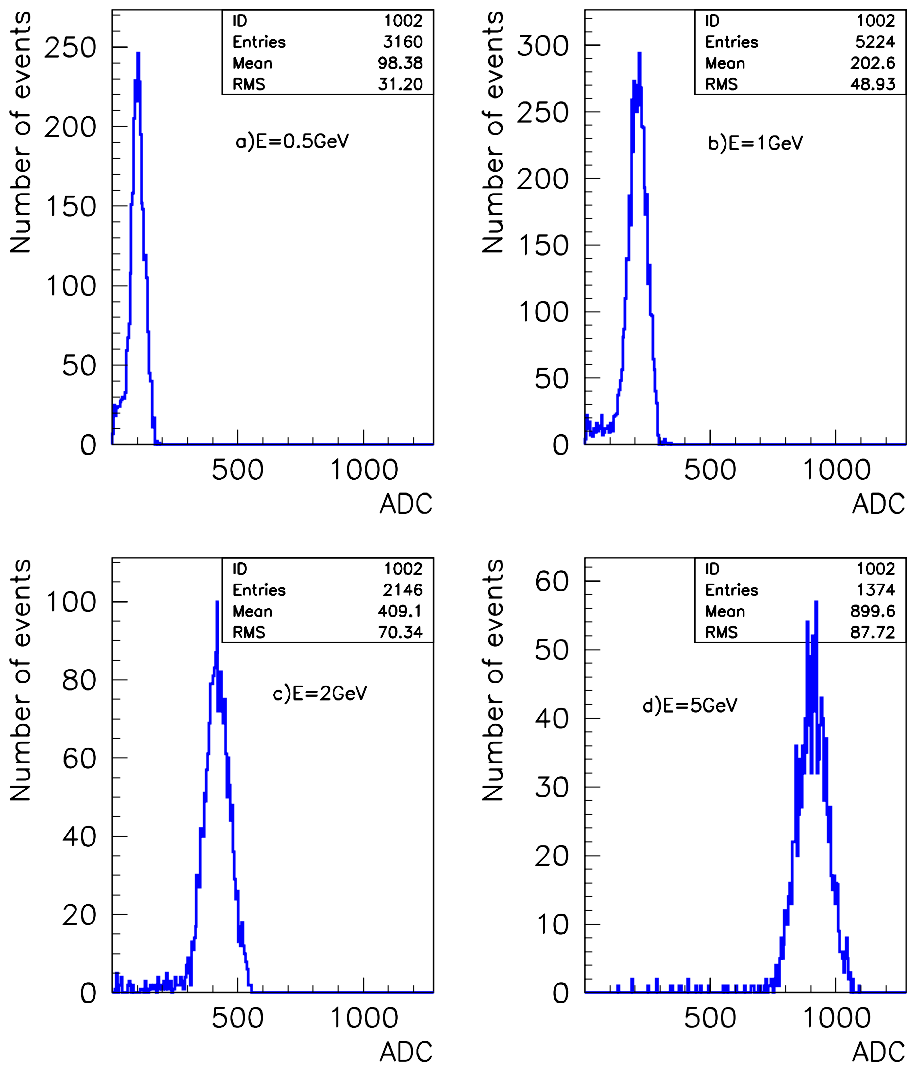

Figure 2: EMC energy response to electron in ADC counts at four energies: a) 0.5 GeV ; b) 1 GeV ; c) 2 GeV ; d) 5 GeV.

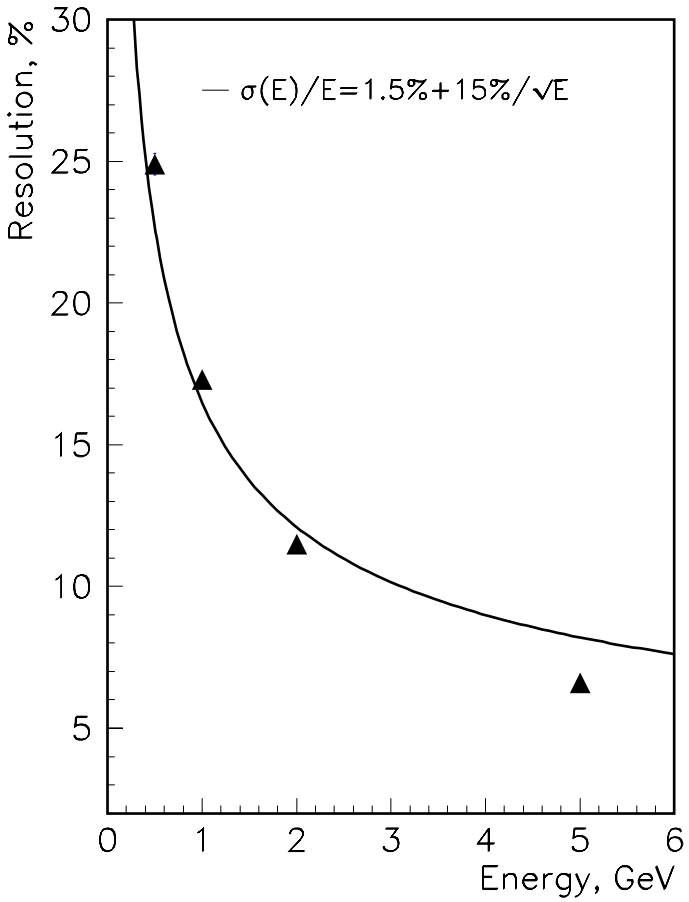

Figure 3: Energy dependence of the EMC energy resolution (sigma for Gaussian fit).

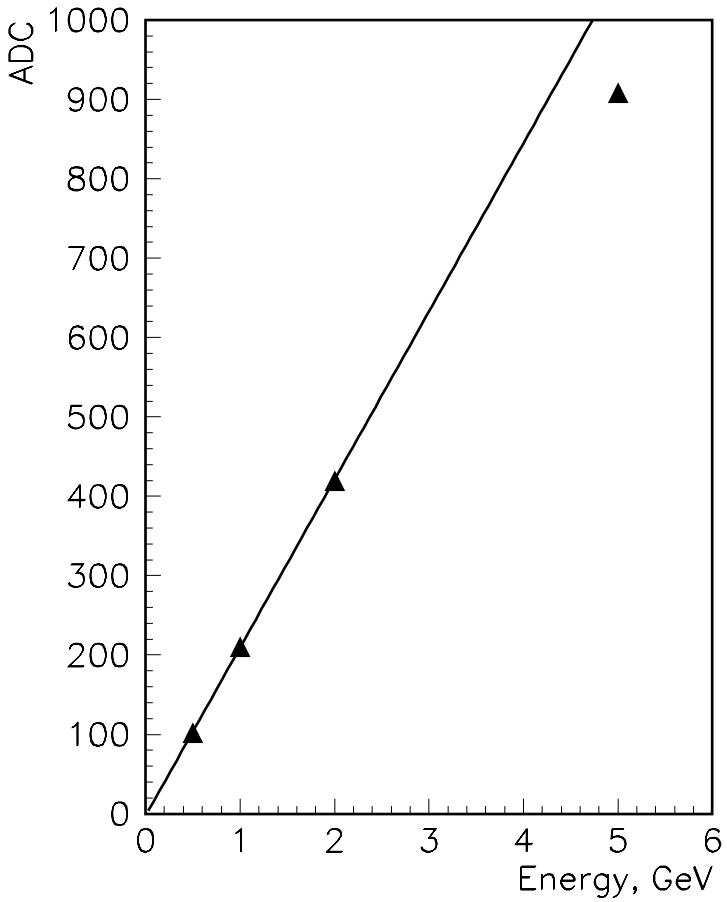

Figure 4: Energy dependence of the EMC response.

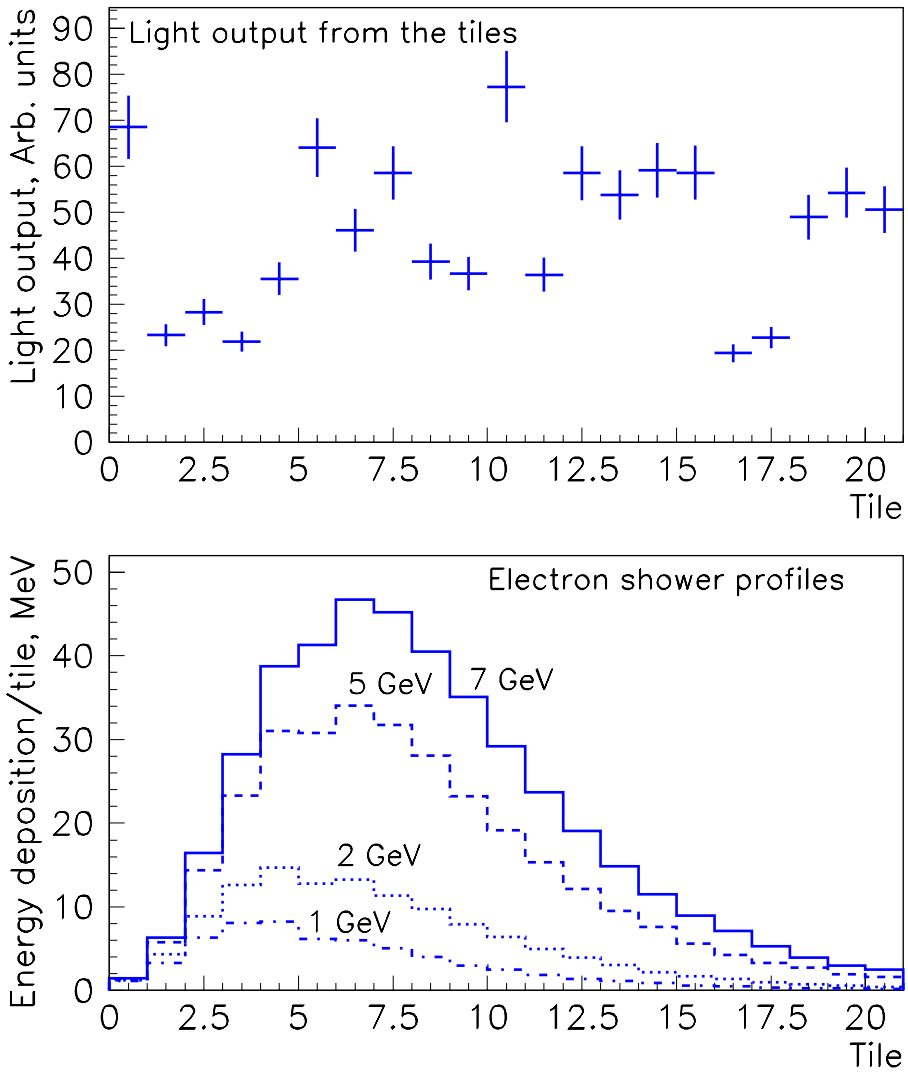

Figure 5: Measured relative light yield from 21 scintillator tiles of Tower 2 (upper frame), and GEANT simulated longitudinal electron shower's profiles (lower frame).

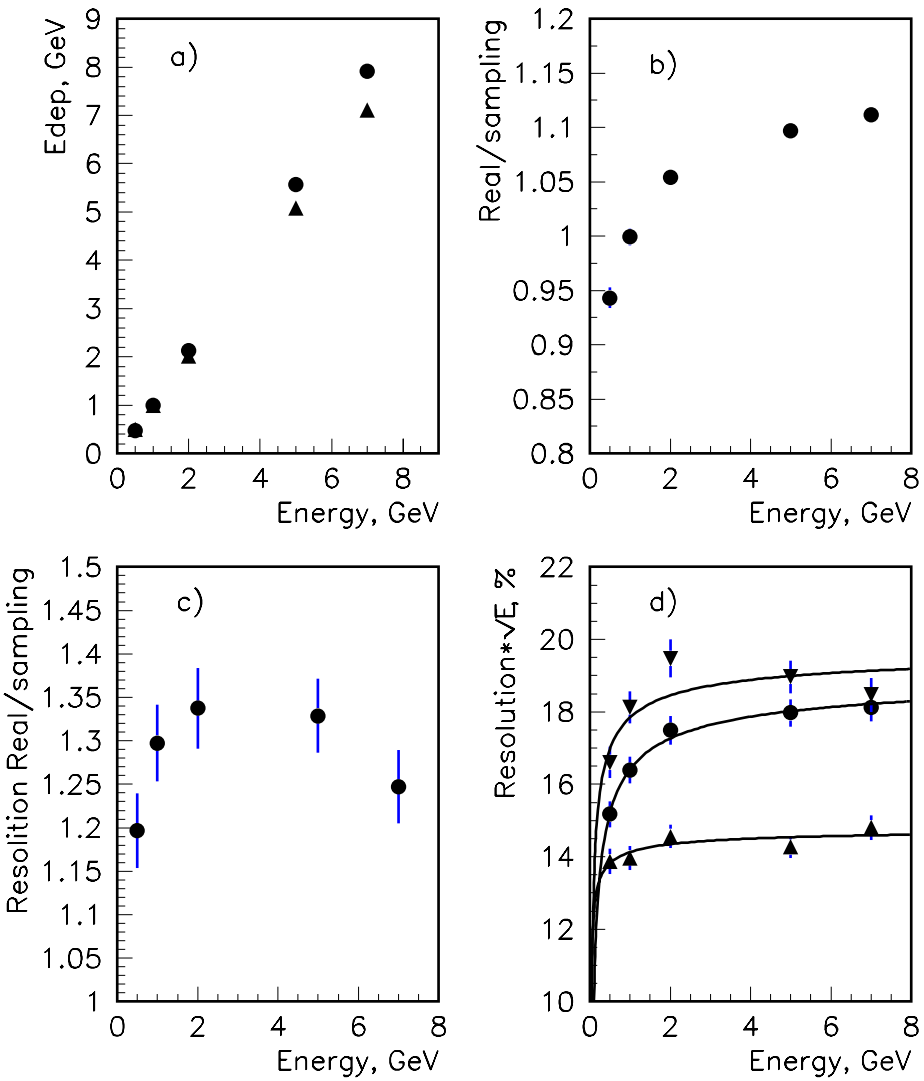

Figure 6: GEANT simulated results with taking into account non-uniformity in tile light output for Tower 2. a) energy dependence of EMC response (triangles - tile light output is supposed to be uniform; circles - real non-uniform tile light output); b) ratio of two energy EMC responses : with non-uniformity to uniform tile light output; c) ratio of energy resolutions for the case b); d) energy resolution times $\sqrt{E}$.

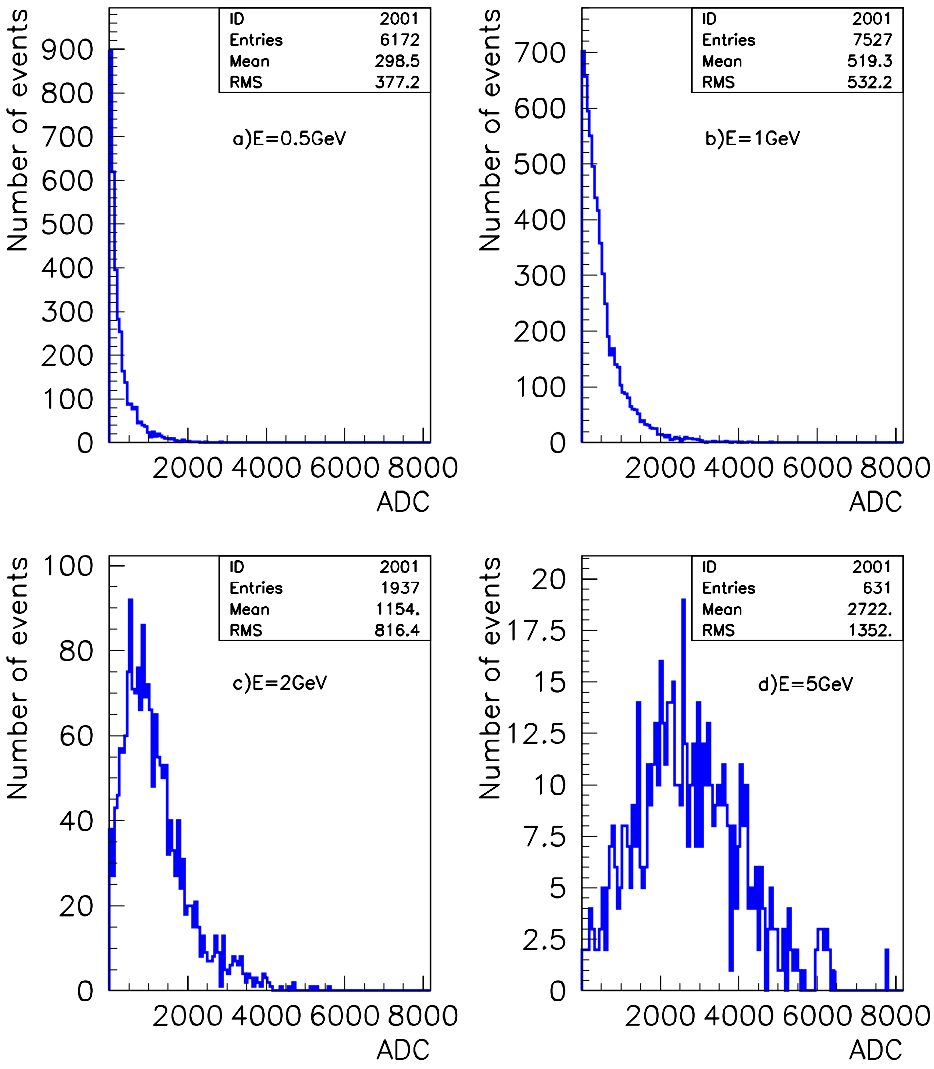

Figure 7: SMD energy response in ADC counts for electrons at four energies: a) 0.5 GeV ; b) 1 GeV ; c) 2 GeV ; d) 5 GeV.

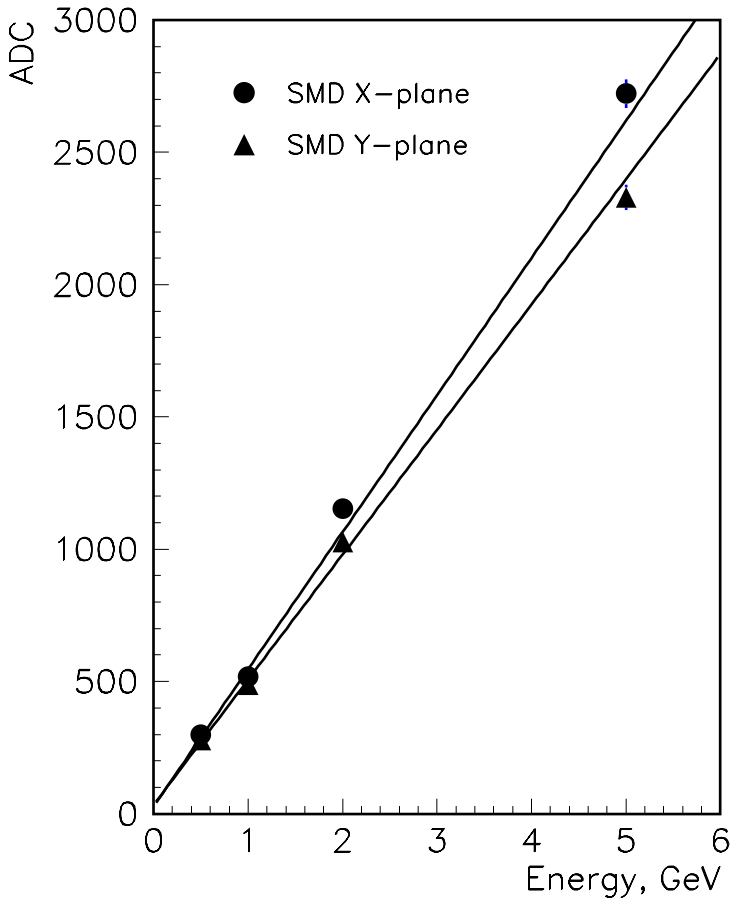

Figure 8: Energy dependence of the mean SMD signal.

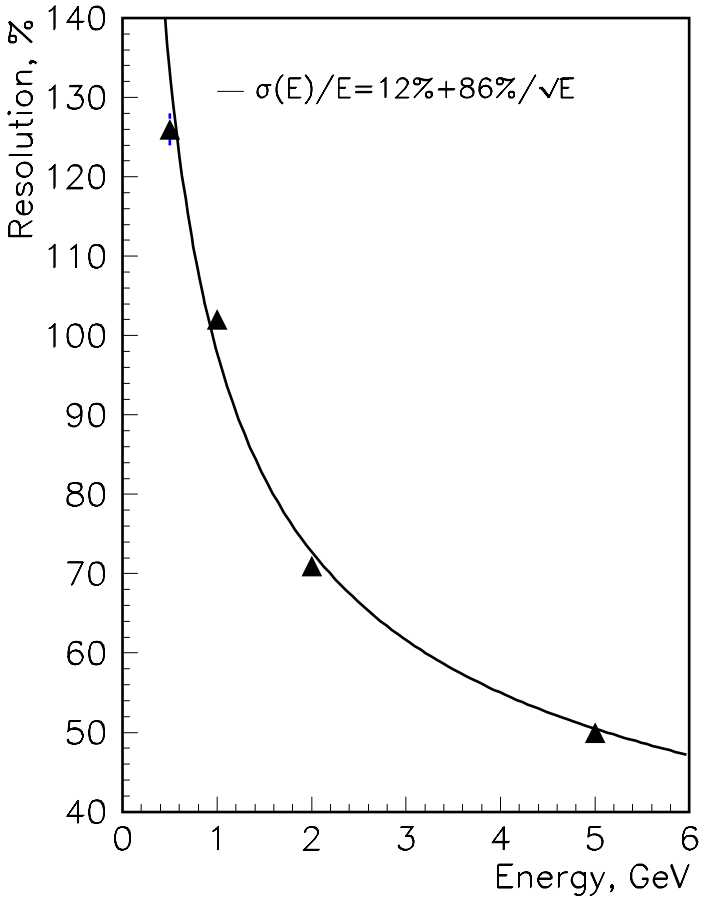

Figure 9: Energy dependence of the SMD energy resolution.

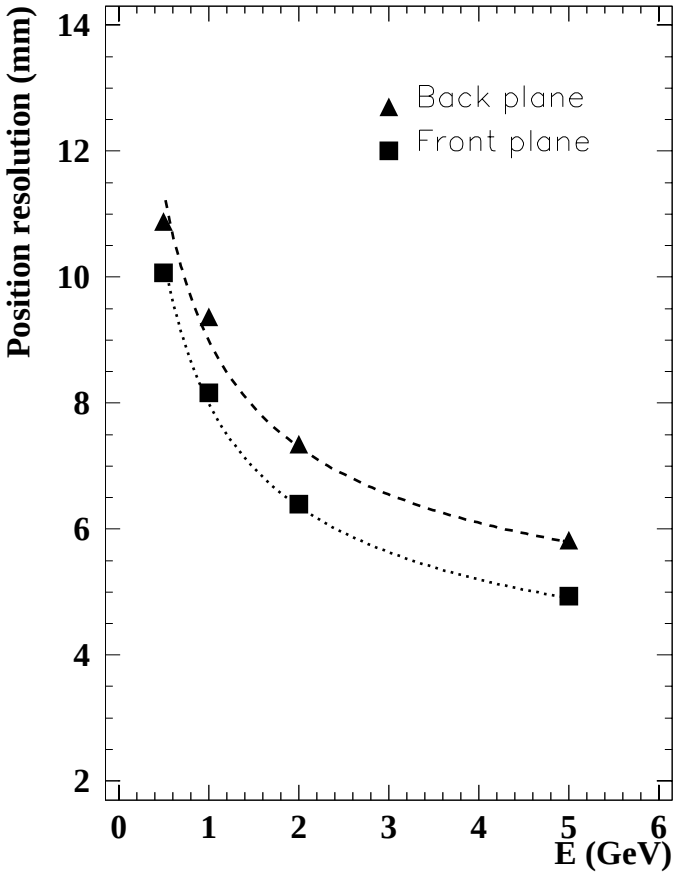

Figure 10: Position resolution for electrons in the SMD's front and back planes.

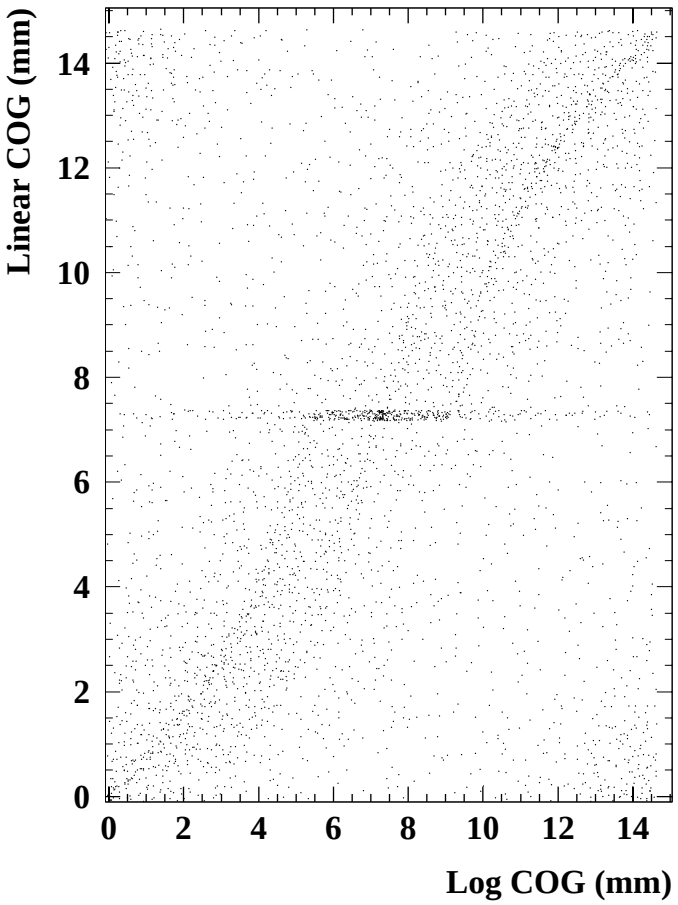

Figure 11: The position of the 5 GeV shower axis as determined by the linear weighted method vs logarithmic algorithm, for a uniformly distributed impact parameter across the strip surface.

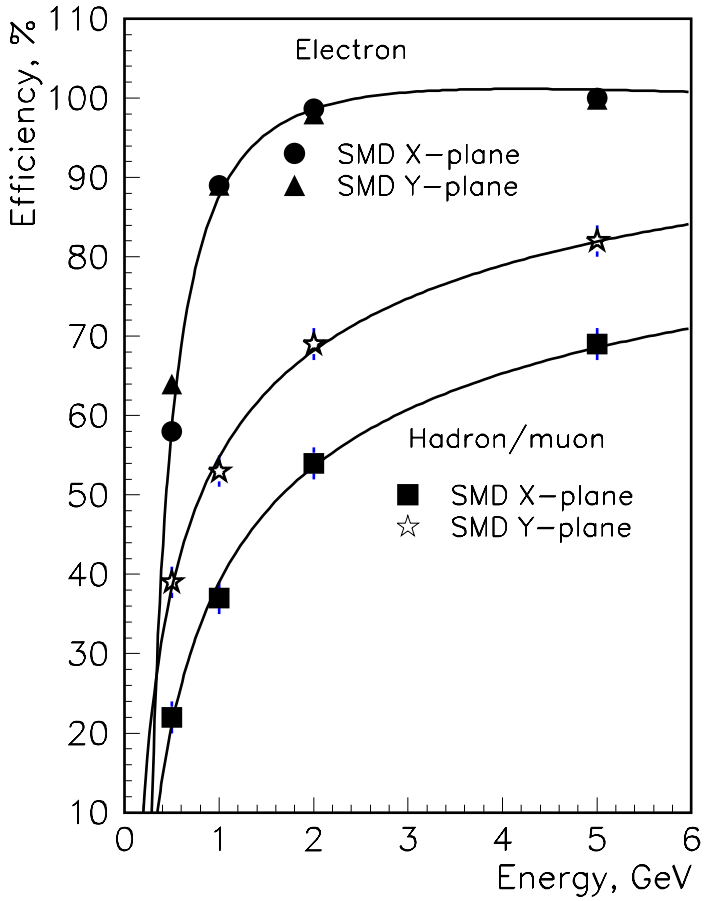

Figure 12: Electron and hadron/muon detection efficiencies in the SMD.

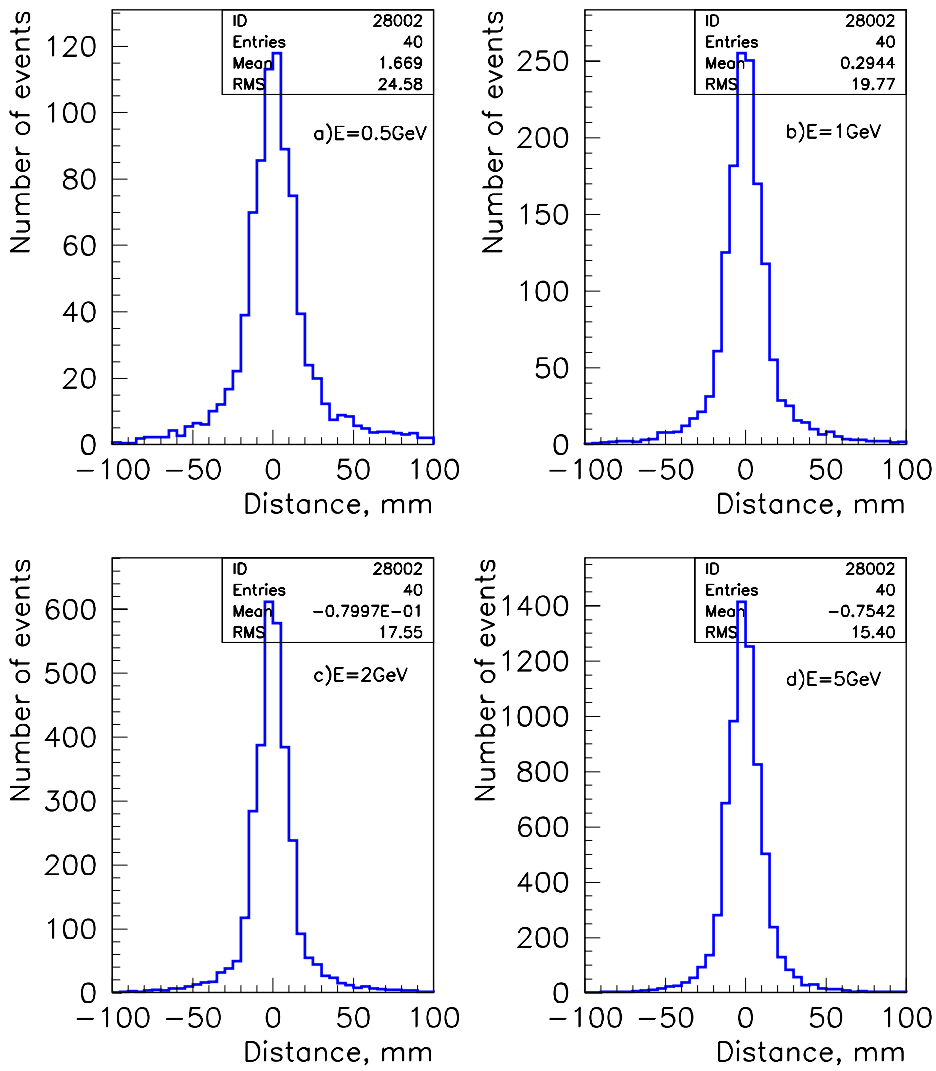

Figure 13: The measured SMD transverse shower profiles for electrons at the energies: a) 0.5 GeV ; b) 1 GeV ; c) 2 GeV ; d) 5 GeV.

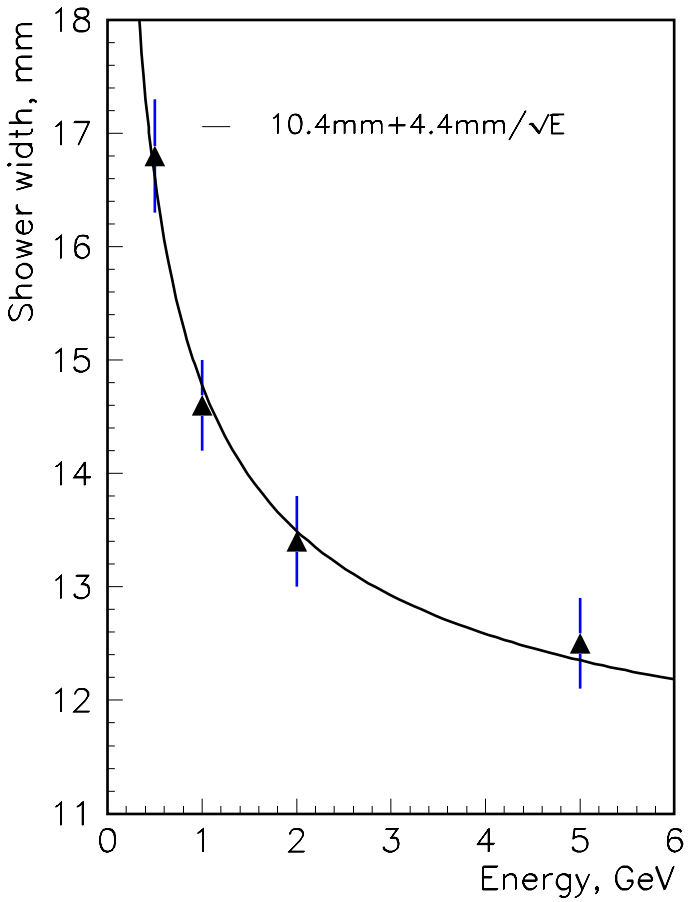

Figure 14: Energy dependence of the electron shower width in the SMD. Shower profile width is RMS of the shower profile (see. Fig.14) in the range from -50 to 50 mm.

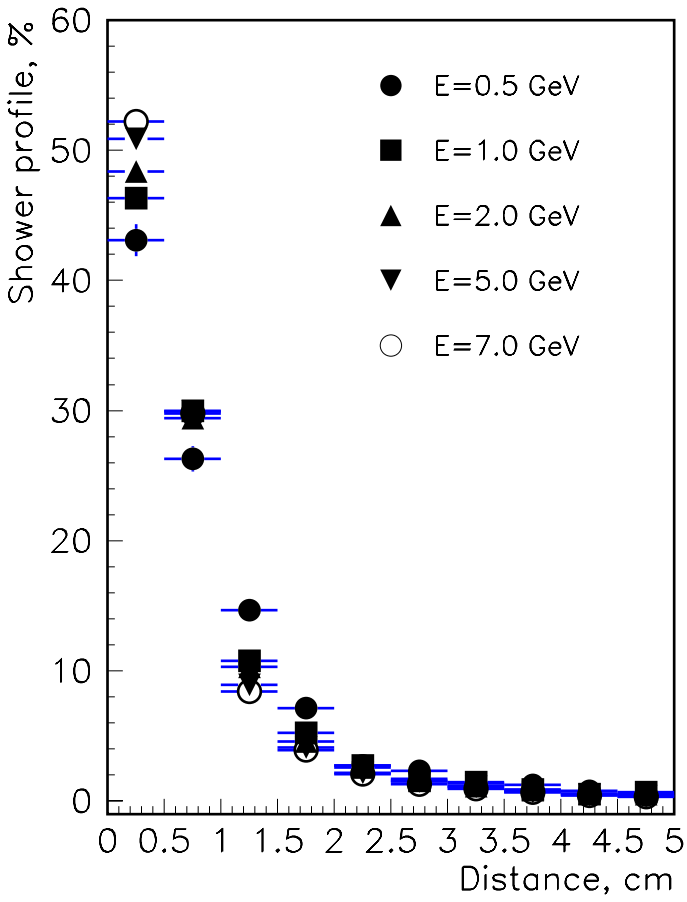

Figure 15: GEANT simulated transverse shower profiles in the SMD for electrons of various energies.

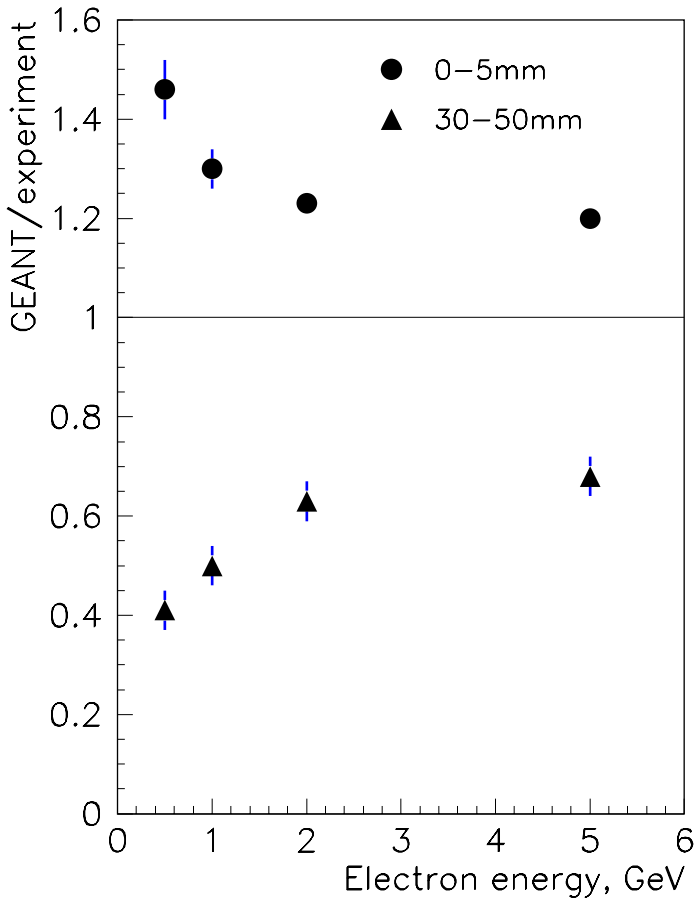

Figure 16: Ratios of the GEANT simulated fraction of the shower profiles to the measured fractions at two distances from the beam axis : 0 to 5 mm, and 30 to 50 mm.

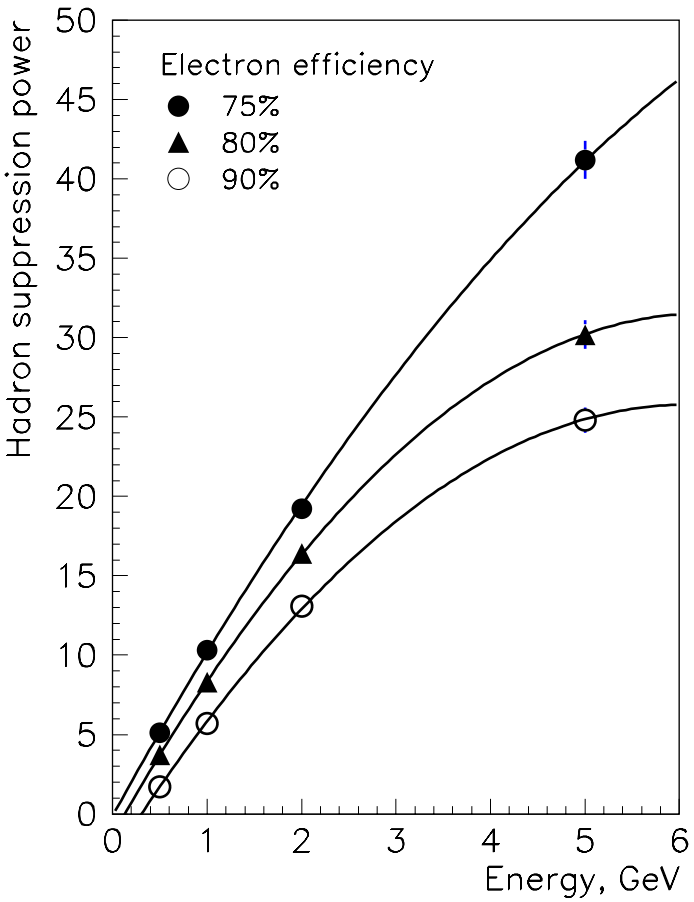

Figure 17: The hadron suppression power, using only the EMC, for three different values of the electron detection efficiency.

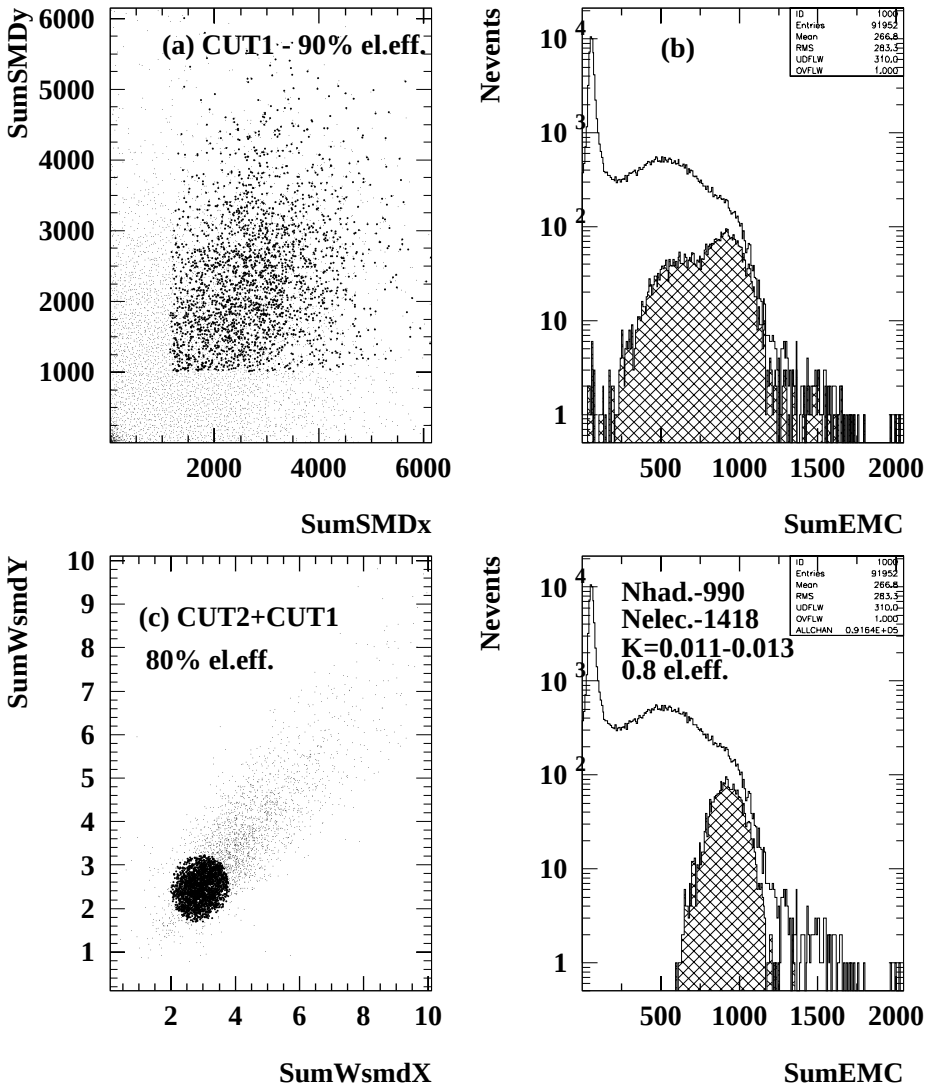

Figure 18: a) the single-sided cuts applied for the front and back SMD planes to identify 5 GeV electrons with 90% efficiency; b) the amplitude spectra in the EMC for the entire data sample and surviving events (hatched) after applying cuts in the SMD; c) the distribution of the ratio of the sum of the strip logarithmic weights over energy deposition in the EMC for the front vs back planes of the SMD for the events surviving the first cuts, and applied cut to identify electrons with 80% efficiency; d) the amplitude spectra in the EMC for the events surviving after all applied cuts (hatched) as well as for the entire data sample.